Direct Evidence for Buffer-Enhanced Proton-Coupled Electron Transfer in Metal Aquo Bond Formation

Matthew Kessinger[†], Thomas Whittemore[†], Silvia Grandi[§], Evgeny Danilov[‖], Stefano Caramori[§], Felix Castellano[‖], Gerald Meyer[†]

[†] Department of Chemistry, The University of North Carolina at Chapel Hill, Chapel Hill, NC, USA

[§] Department of Chemical, Pharmaceutical and Agricultural Sciences, Ferrara, Italy

[‖] Department of Chemistry, North Carolina Sate University, Raleigh, NC, USA

Keywords: Proton-coupled electron transfer, transient absorption, spectroscopy, kinetics, mechanism, interfaces

Abstract

Proton-coupled electron transfer (PCET) reactions play a crucial role in the interconversion of metal-aqua and metal-hydroxo species present in transition metal complexes and oxide surfaces (M^{III}-OH + e^- + H^+ → M^{II}-OH_2). For ruthenium-based water oxidation catalysts, PCET reactions involved in the mechanism of O_2 evolution have demonstrated a strong dependence on the identity and concentration of the proton donor and acceptor with significant rate enhancements observed for electrocatalysis performed in acetate, phosphate, and borate buffered electrolytes. However, the systematic study of this phenomenon has been hampered by the inability to independently measure discrete rates for electron transfer (ET) and proton transfer (PT) under electrochemical applied potentials. Herein, the PCET kinetics and mechanism of metal aqua bond formation in a ruthenium water oxidation catalyst $[Ru^{II}(tpy)(bpy')H_2O]^{2+}$, $Ru^{II}-OH_2$ where tpy is 2,2′:6′,2″-terpyridine and bpy′ is 4,4′-diaminopropylsilatrane-2,2′-bypyridine were investigated at a conductive metal oxide interface as a function of buffer identity and concentration. The reaction of interest was triggered by visible light excitation of the catalyst and the kinetics of the independent ET and PT steps of the PCET mechanism were determined through nanosecond transient absorption spectroscopy. Kinetic measurements performed in aqueous acetate, phosphate, or borate buffer solutions revealed two distinct regimes of PT kinetics solely dependent on the buffer concentration. At the greatest buffer concentrations investigated (2 M acetate) spectral signals corresponding to the discreet ET and PT steps were absent indicative in a change in underlying PCET mechanism. Likewise, kinetic modeling indicated that PT from protonated acetate or phosphate occurred with rate constants that were 2-4 orders of magnitude greater than those for bulk water. In all, these results suggest that the presence of buffer-bases can significantly enhance PCET rates and, in this reaction, may alter the underlying mechanism.

Introduction

Proton-coupled electron transfer (PCET) reactions underpin many of the fuel-forming processes found within natural and artificial photosynthesis.[1–9] For catalytic applications in artificial photosynthesis, the proton transfer (PT) step of PCET may be mediated by various sources such as protic solvents, exogenous acids, and inorganic or organic buffer-bases. While linear free-energy relationships for PCET reactions performed in the presence of secondary acid sources and organic buffer-bases are well-known in many organic solvents,[10–18] the influence of

buffer-bases on the kinetics and mechanisms of PCET reactions performed in aqueous solutions is considerably more difficult to resolve due to solvent participation in the PCET reaction. Several reports of buffer-enhanced PCET in aqueous solutions have focused on the performance of electrocatalysts used for water oxidation,[19–22] hydrogen evolution,[23–27] and carbon dioxide reduction.[28] Often times, enhancements in the catalytic current or onset potential is attributed to direct involvement of the buffer-base in the rate-determining step of the catalytic cycle.[29] In addition, computational modeling has supported the preference for some PCET reaction centers to favor dissolved buffer-bases over bulk solvent as a preferred proton acceptor.[30] Other studies suggested that the presence of buffer-bases may lead to alternative mechanistic pathways with unique thermodynamic or kinetic requirements.[31]

For molecular water oxidation catalysis, the addition of buffer-bases has been shown to enhance the electrocatalytic performance of ruthenium,[19] cobalt,[21] and nickel[20] water oxidation catalysts. Such enhancements were attributed to a concerted EPT mechanism mediated by the buffer-base that lowers the activation barrier for rate-limiting O−O bond formation.[32] In a recent report on HER performed via a cobalt-porphyrin peptide assembly, the influence of buffer pH, acid dissociation constant (pK_a), and concentration of a suite of organic buffer-bases was investigated. The authors discovered that the catalytic half-wave potential was dependent on the buffer pK_a.[25] In the presence of buffers with a pK_a < 7.7, a mechanistic switch was invoked wherein buffer participation in rate-determining Co(III) hydride formation led to enhanced catalytic performance. Finally, others have demonstrated that small, cationic buffer-bases featuring organic heteroatoms have shown promise for enhancing CO_2 reduction catalysis in nickel cyclam catalysts.[28] Interestingly, the use of small inorganic buffer-bases such as carbonate or phosphate led to preferential binding of the base to catalytic centers that enhanced H_2 evolution relative to CO_2 reduction. These studies clearly demonstrate that the addition of buffer-bases can dramatically alter the kinetics and mechanisms of PCET reactions.

While prior studies have relied on electrochemical methods[33–35] to establish the activity of buffer-bases towards enhancing PCET reactions, they often lack the time resolution necessary to track the independent electron transfer (ET) and PT steps within a PCET mechanism. As a result, the study of PCET reactions with techniques capable of sub-millisecond time resolution promises to greatly extend our understanding of buffer-base effects. In particular, the use of time-resolved spectroscopy to trigger and isolate the individual steps of chemical mechanisms has demonstrated the potential to provide an enriched understanding of buffer-enhanced PCET reactions. Surprisingly, there are few reports of photo-induced PCET reactions that examine the impact of dissolved buffers on aqueous PCET kinetics using time-resolved spectroscopy. One notable example provided by Hammarström examined the photo-oxidation of tyrosine by a ruthenium photosensitizer in a PCET donor-acceptor moiety. The PCET kinetics were measured at fixed pH values in the presence of phosphate buffer.[36] Notably, two kinetic regimes were observed where at low buffer concentrations, the rate of tyrosine oxidation was found to be independent of buffer concentration. However, at elevated concentrations of phosphate buffer, a kinetic enhancement was observed. These two regimes were assigned to PCET where either bulk solvent (low buffer concentrations) or the dissolved buffer-base (high buffer concentrations) served as the proton acceptor. Ultimately, the kinetic enhancement was attributed to the onset of concerted EPT between tyrosine and the dissolved buffer.[36] While this study is instrumental in providing evidence of buffer-base effects operating within aqueous light-driven PCET, there have been no studies to date of buffer-enhanced PCET kinetics where the independent ET and PT steps were kinetically resolved. Furthermore, studies of buffer-base effects on light-initiated PCET

reductions have been critically absent from the literature, prompting the need for further investigation.

Within the vast array of PCET reactions, the reduction of a metal hydroxo species to yield a metal aquo species (M_{OX}−OH + e^- + H^+ → M_{red}−OH_2) underscores many critical processes found in environmental, biological, and inorganic chemistry.[18,37–41] Recently, our groups reported a surface-anchored single-site ruthenium water oxidation catalyst, $[Ru^{II}(tpy)(bpy')OH_2]^{2+}$ where tpy = 2,2′:6′,2″-terpyridine and bpy′ is 4,4′-dimainopropylsilatrane-2,2′-bipyridine (Ru^{II}−OH_2) immobilized on mesoporous tin-doped indium oxide (InO_2:Sn, ITO) thin films.[42] Under visible light excitation, electron injection into ITO coupled with deprotonation of the aquo ligand leads to the selective formation of $[Ru^{III}(tpy)(bpy')OH]^{2+}$ (Ru^{III}−OH). On nanosecond and longer timescales, reduction of the catalyst coupled with proton transfer from solution resulted in the regeneration of Ru^{II}−OH_2 **(Scheme 1, left**). The application of an applied potential (V_{app}) to the ITO thin films afforded direct control over the driving force (−Δ*G*°) for electron transfer. Under sufficiently negative V_{app} (≤ −0.1 V *vs.* NHE), spectroscopic signals corresponding to the independent electron transfer (ET) and proton transfer (PT) steps provided a definitive mechanistic assignment of stepwise ET-PT with rate-limiting proton transfer. The ability to kinetically resolve rates of both ET and PT provides a unique opportunity to study the impact of buffer-bases on the kinetics and mechanisms of stepwise ET-PT for metal-hydroxide reduction.

Scheme 1. (Left) Stepwise PCET Reduction of Ru^{III}−OH; (Right) Buffer-Enhanced PCET Reduction of Ru^{III}−OH.

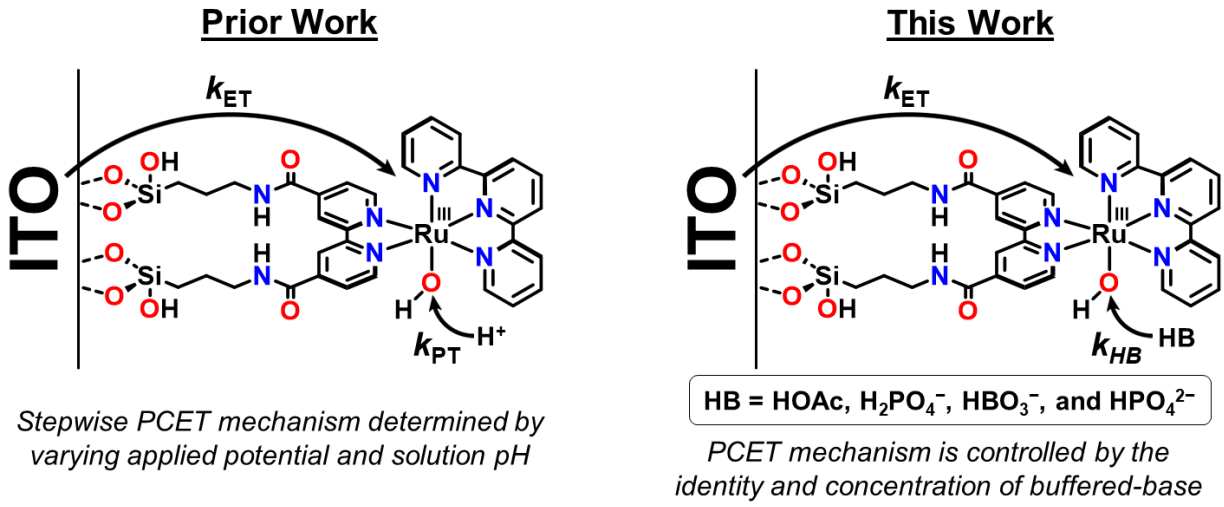

Stepwise PCET mechanism determined by varying applied potential and solution pH

PCET mechanism is controlled by the identity and concentration of buffered-base

Herein, we report the buffer-enhanced PCET reduction of Ru^{III}−OH to yield Ru^{II}−OH_2. Kinetic data were collected in variable concentrations of either acetate or phosphate buffered electrolytes at constant solution pH (**Scheme 1, right**). At low buffer concentrations, rate constants for ET and PT were independent of the dissolved buffer concentration. However, at elevated buffer concentrations, a prominent enhancement in the PT rate constant was observed. Rate constants for ET were relatively insensitive to the concentration of buffer. At concentrations in excess of 500 mM for both buffers, spectral signals corresponding to the formation of the one-electron reduced intermediate were absent from nanosecond transient absorption spectra suggesting a change in the underlying PCET mechanism from ET-PT with rate-limiting PT to ET-PT with rate-limiting ET or concerted electron-proton transfer (EPT).

Experimental Methods

Materials. All chemicals and reagents were purchased from either T.C.I., MilliporeSigma, Acros Organics, Ambeed, or VWR and used as received without additional purification. Conductive tin-doped indium oxide (ITO) nanoparticles (~40 nm diameter, <10% doping) were purchased from Inframat Advanced Materials and used as received. Samples of $[Ru^{II}(tpy)(bpy')Cl]Cl$ were prepared following previously reported methods[42] and were allowed to adsorb to ITO thin films before conversion to the aqua species. Colloidal solutions of either zirconium oxide (ZrO_2) or ITO were prepared using literature methods.[42,43]

Solution pH Measurements. The solution pH was measured using an Acumet AB15 digital pH meter (Fisher Scientific) calibrated beforehand with standard buffer solutions at pH = 4.01, 7.00, and 10.01. For transient absorption spectroscopy, all buffered electrolyte solutions consisted of either phosphate buffer prepared by dissolving disodium hydrogen phosphate heptahydrate and sodium dihydrogen phosphate monohydrate (1.31-to-1.0 mol ratio) in water or by dissolving sodium acetate in water to prepare solutions with total buffer concentrations of 0.1 mM, 0.3 mM, 0.5 mM, 1 mM, 5 mM, 50 mM, and 500 mM. Sodium perchlorate was added to each electrolyte solution to provide a constant ionic strength (μ = 0.54 for phosphate and μ = 0.50 for acetate). The necessary ionic strength was calculated based on the ionic strength of a 500 mM buffered electrolyte solution. The solution pH was then adjusted where necessary using solutions of NaOH and $HClO_4$. The concentration of acid or base used was varied to result in the least amount of sample dilution. In addition, 2 M acetate buffer solution (pH 5.5) and 800 mM phosphate buffer solution (pH 7) were also prepared to test the extreme ranges of buffer concentration.

Electrochemical Measurements. Cyclic voltammetry was performed in a three-electrode cell with a sensitized ITO thin film as the working electrode, a Ag/AgCl (3 M NaCl) reference electrode, and a Pt mesh counter electrode. Before and after each experiment, the Ag/AgCl electrode was referenced to a saturated calomel electrode (SCE = +241 mV vs. NHE)[44] by connecting both electrodes to a voltmeter and immersing them in an aqueous 3 M NaCl solution. The measured reference potential was found to be −31 ± 5 mV vs. SCE for all measurements. If a deviation in the reference potential was observed outside of this range, the Ag/AgCl reference electrode was remade and allowed to equilibrate for 3 days prior to use. Where necessary, the reference potentials were converted from Ag/AgCl to NHE using the relationship provided above and the measured reference potential versus SCE. The applied potential (V_{app}) was controlled using a CHI 601D potentiostat. All plots of the electrochemical data are provided using the polarographic convention.

Absorption Spectroscopy. Ultraviolet (UV) – visible absorption spectroscopy was performed on a Cary 60 UV-Vis absorption spectrometer. A Teflon insert placed inside a standard 1 cm^2 cuvette was used to hold the ITO thin film electrodes at a fixed angle of 45°. Before taking spectroscopic measurements, a spectrum of the bare FTO slide immersed in the electrolyte solution was saved as a blank. Measurements were collected across the visible spectrum before and after each transient absorption experiment. The films showed no obvious signs of degradation with absorption maxima between measured before and after pulsed laser excitation within 5% of each other. Where necessary, a separate spectrum of the bare ITO thin film was measured and manually subtracted from the absorption spectrum of the dyed electrodes to provide clearer spectral features.

Transient Absorption. All transient absorption experiments were carried out in argon-saturated aqueous solutions of either acetate or phosphate buffer. During the spectroscopic measurements argon was allowed to flow continuously into the headspace of the cell to prevent oxygen from

leaking into the sample solution over the course of the measurements. Transient absorption spectroscopy with nanosecond time resolution was performed in a standard three electrode cell prepared into a standard 1 cm^2 glass cuvette fitted with a 24/40 ground glass joint. A rubber septum was modified with custom electrochemical leads to provide access to the working, counter, and reference electrodes inside the cuvette. The working electrode consisted of a ITO slide with surface-anchored catalyst oriented at a 45° angle to the incident laser beam, a Ag/AgCl (3 M) reference electrode and a Pt-mesh counter electrode. Varying applied potentials were controlled using a CH1 601D potentiostat from CH Instruments. Samples were allowed to equilibrate for 10-30 seconds upon the application of each applied potential until the relative current response had returned to baseline.

Pulsed excitation of each sample was accomplished using a RADIANT X30 tunable laser system: Q-switched, pulsed (10Hz) Nd:YAG laser (Quantel laser By Lumibird, Q-smart 450mJ) tripled to 355 nm, coupled with an OPO module (410-2500 nm tuning range). The laser fluence at the sample was 2.5-5.0 mJ/pulse at 488 nm. A 450 W xenon arc lamp aligned perpendicular to the laser served as the probe beam. Two shutters placed between the arc lamp / laser and the sample were pulsed at 10 Hz to limit PMT fatigue and sample degradation. The probe light was focused onto the sample, collimated after the sample, and focused onto an Oriel Cornerstone 260 monochromator optically coupled to a Hamamatsu R928 photomultiplier tube. The transient signal was recorded with a Teledyne Lecroy Wavesurfer 4024HD, 200 MHz digital oscilloscope (with variable bandwidth filters to improve the signal-to-noise ratio). The laser flashlamps, Q-switch, shutters, and oscilloscope trigger delays were controlled with a Berkley Nucleonics Corp. Model 577 Digital Delay Generator. Single-wavelength kinetics were generated as an average of 150 laser shots to achieve adequate signal-to-noise ratios. Each experimental average consisted of one spectrum obtained in the absence of pulsed laser excitation and one spectrum obtained immediately following pulsed laser excitation (14 ns instrument response time). The difference between these two spectra were saved and averaged.

Kinetic Modeling. A detailed explanation of the kinetic model and a table of the best fit parameters is provided in the supporting information.

Results.

Colloidal suspensions of tin-doped indium oxide (In_2O_3:Sn, ITO) or zirconium oxide (ZrO_2) nanoparticles were coated onto conductive glass substrates and heated under an oxygen atmosphere to provide the high surface area mesoporous thin films utilized for interfacial studies. Thin films containing the surface-anchored catalyst were prepared by isolation and immobilization of the pre-catalyst, $[Ru^{II}$(2,2′:6,2″-terpyridine)(4,4′-diaminopropylsiltrane-2,2′-bipyridine)Cl$]^{2+}$, to the electrode surface as previously reported.[42] Incubation of these electrodes in 50 °C aqueous solutions for 72 hours provided sufficient time for ligand exchange *in situ* to yield thin films of the desired catalyst, $[Ru^{II}$(2,2′:6,2″-terpyridine)(4,4′-diaminopropylsiltrane-2,2′-bipyridine)$OH_2]^{2+}$, $Ru^{II}-OH_2$. The acid dissociation constants (pK_a) and formal potentials (E°) for $Ru^{II}-OH/OH_2$ and $Ru^{III}-OH/OH_2$ immobilized at an ITO interface have been previously reported and are provided for reference in **Table S1**. **Figure 1** shows the ultra-violet (UV)-visible absorption spectrum of catalyst sensitized ZrO_2 thin films collected in 5 mM phosphate buffer solutions adjusted to pH 7 and pH 12. Both samples are characterized by an intense metal-to-ligand charge transfer (MLCT) absorption band located in the visible region of the spectrum at 495 nm and 540 nm, respectively. Deprotonation of the aqua ligand at pH > pK_a = 10.3 results in the formation of $Ru^{II}-OH$ and produces a bathochromic shift in the MLCT absorption, consistent with prior reports for this catalyst.[42,45] The surface coverage (Γ) of $Ru^{II}-OH_2$ was determined spectroscopically using a modified form of the Beer-Lambert law[46–48]

$$\Gamma = \frac{A}{1000 \times \varepsilon} \quad (1)$$

Where *A* is the intensity of the MLCT absorption maximum and ε is the molar extinction coefficient (ε_{max} = 9600 M^{-1} cm^{-1})[48]. Values of Γ varied between 3.8 × 10^{-8} mol/cm^2 and 8.3 × 10^{-8} mol/cm^2 in agreement with prior reports for sensitized mesoporous metal oxide electrodes.[43,46–49]

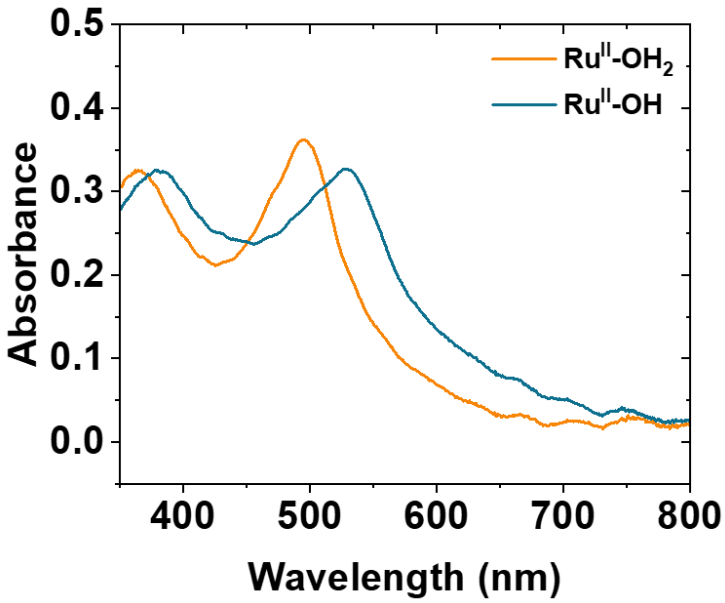

Figure 1. UV-visible Absorption profiles of Ru^{II}−OH2 (orange trace), Ru^{II}−OH (blue trace).

Figure 2 shows the electrochemical response of ITO thin films containing surface-anchored Ru^{II}−OH_2 in 500 mM solutions of either pH 5.5 acetate buffer or pH 7.0 phosphate buffer. The cyclic voltammograms are characterized by broad quasi-reversible waves with peak currents that were approximately equal in amplitude and a peak-to-peak splitting greater than 60 mV. The formal potential (*E*°) was calculated from the average of the anodic and cathodic peak potentials. These values were found to be +0.924 *V vs* NHE and +0.822 *V vs* NHE for acetate and phosphate buffer solutions, respectively. A shift to more negative potentials in more alkaline conditions is explained by the reported PCET reactivity of this catalyst across the indicated pH range.[42,43,45,50]

Cyclic voltammograms of the surface-anchored catalyst collected as a function of buffer concentration are provided in **Figure S1**. Prior reports noted that aqueous solutions of a related ruthenium-based water oxidation catalyst measured in >50 mM acetate buffer solutions displayed a pH-independent electrochemical response that was attributed to displacement of the inner-sphere H_2O for acetate.[32] To determine if ligand exchange was present for thin films of Ru^{II}−OH_2, samples were allowed to equilibrate in 2 M acetate buffer solution between pH 3.5 and 5.0 for 30 minutes prior to electrochemical cycling. This incubation time was selected as it was the average duration necessary to perform a typical time-resolved kinetic measurement. The results are provided in **Figure S2**. In contrast to previous reports, the cyclic voltammograms display a cathodic shift of 55 mV/pH unit under increasing alkalinity that are consistent with preserved

PCET reactivity on the timescale of the electrochemical and spectroscopic measurements performed herein.

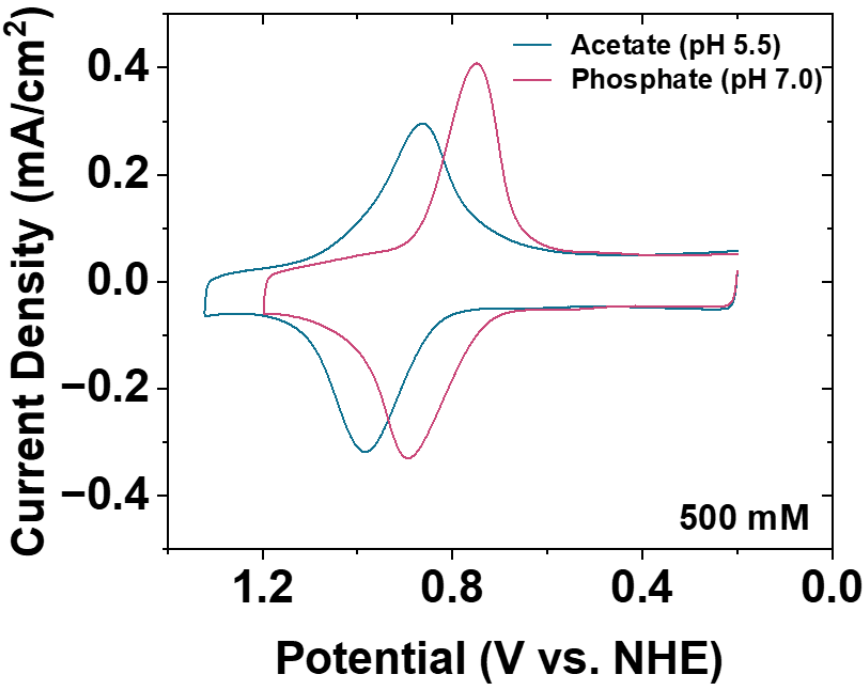

Figure 2. Cyclic voltammogram of surface-anchored $Ru^{II}-OH_2$ collected at 10 mV/s in 500 mM buffered electrolyte solutions of either pH 5.5 acetate buffer (blue) or pH 7.0 phosphate buffer (pink).

Photoexcitation of surface-anchored $Ru^{II}-OH_2$ under a constant applied potential (V_{app}) resulted in rapid electron injection into ITO and generation of $Ru^{III}-OH$, consistent with prior reports for this catalyst anchored to ITO.[42,43,48] On microsecond and longer timescales, electrochemical reduction and protonation of $Ru^{III}-OH$ leads to the regeneration of $Ru^{II}-OH_2$. The square scheme provided in **Scheme 2** outlines the potential mechanistic pathways for this PCET reduction reaction.

Scheme 2. Square-Scheme of the Potential Mechanistic Pathways for the PCET Reduction of $Ru^{III}-OH$.

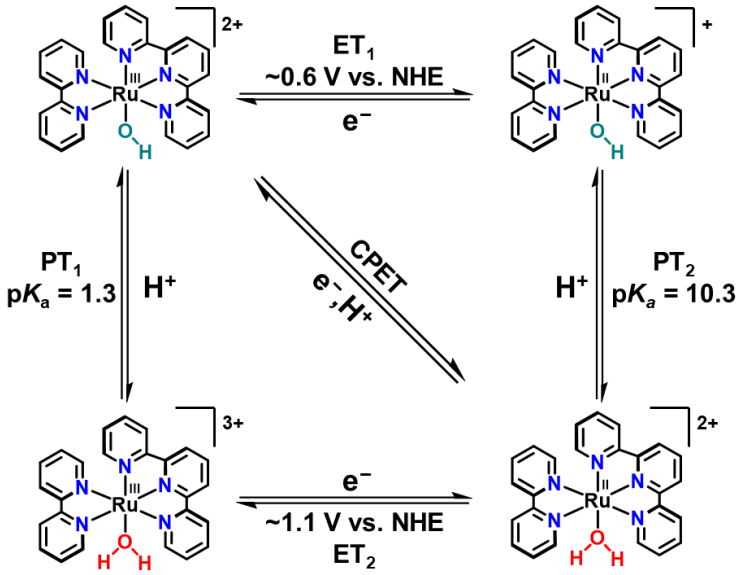

Prior assignment of the operative mechanism in **Scheme 2** suggests that at V_{app} < 0.5 V *vs.* NHE, the PCET reduction of $Ru^{III}-OH$ to yield $Ru^{II}-OH_2$ proceeds through a stepwise electron transfer-proton transfer (ET-PT) mechanism with rate-limiting proton transfer.[42] **Figure 3** displays transient absorption difference spectra collected in pH 5.5 acetate or pH 7 phosphate buffer with a constant V_{app} = -0.1 V *vs.* NHE at varying buffer concentrations. The difference spectra are devoid of spectral features for excited state absorption, consistent with electron injection and deprotonation that occur within the instrument response time of the nanosecond transient absorption apparatus. Within 40 ns of pulsed laser excitation at 488 nm, the difference spectra are characterized by the presence of a prominent ground state bleach centered at 500 nm associated with the oxidation of $Ru^{III}-OH_2$ to yield $Ru^{III}-OH$. A positive growth forms in the spectra by 100 ns and is associated with the initial one-electron reduction of $Ru^{III}-OH$ to yield $Ru^{II}-OH$ (top pathway in **Scheme 2**). On microsecond and longer timescales, both signals decay to the baseline as $Ru^{II}-OH_2$ is regenerated. A simulated transient absorption difference spectrum calculated by modeling the absorptions of $Ru^{II}-OH_2$ and $Ru^{II}-OH$ as a bleach and growth, respectively, is provided in **Figure S3** and supports these spectral assignments. Under elevated buffer concentrations, signals corresponding to the formation of $Ru^{II}-OH$ are weak or absent. Additional transient absorption difference spectra collected at varying buffer concentrations and time delays are provided in **Figures S4-S5**. The absence of spectral features attributed to $Ru^{II}-OH$ suggests that the presence of buffer conjugate acids (CH_3CO_2H and $H_2PO_4^-$) serve as alternative proton sources at elevated buffer concentrations that significantly enhance the rate of PT.

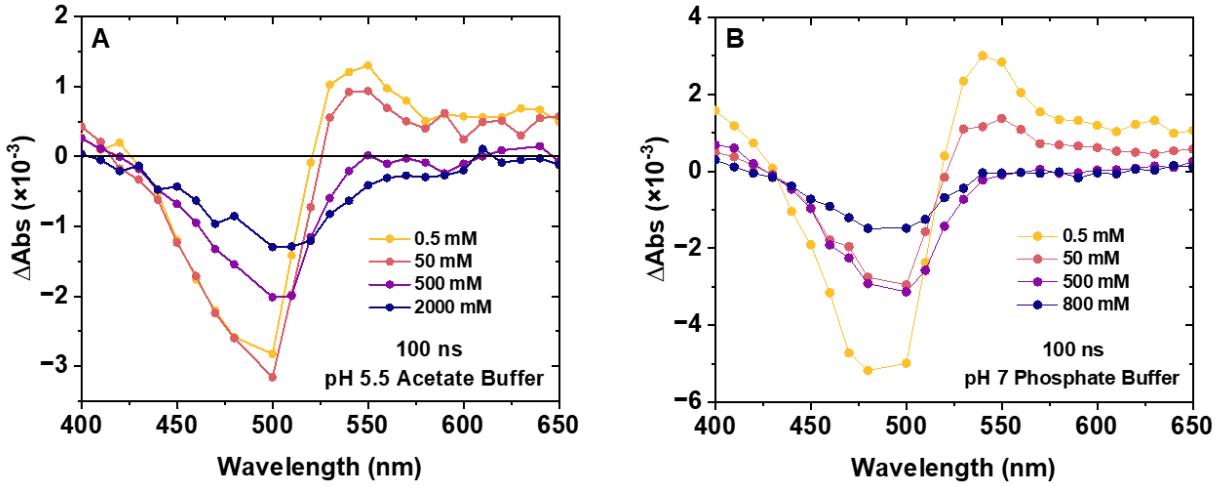

Figure 3. Transient absorption difference spectra collected in acetate (A) or phosphate (B) buffer solutions at varying buffer concentrations and a constant applied potential of −0.1 *V vs.* NHE.

Figure 4 displays single wavelength kinetics measured at 540 nm collected across acetate and phosphate concentrations ranging from 0.1 mM to 2000 mM and 0.1 mM to 800 mM, respectively. As the signal at 540 nm corresponds to the proton transfer reaction, Ru^{II}−OH + H^+ → Ru^{II}−OH_2, the data in Figure 5 clearly suggests a strong kinetic enhancement at buffer concentrations greater than 5 mM.

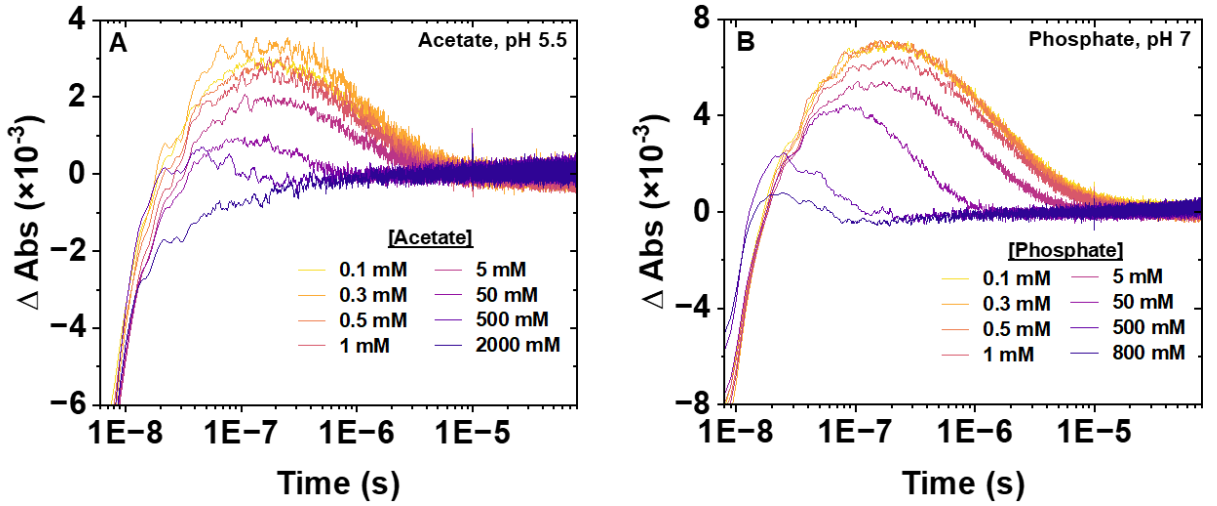

Figure 4. Kinetics collected at 540 nm for the formation and decay of Ru^{II}−OH at the indicated buffer concentrations in either pH 5.5 acetate buffered electrolyte (A) or pH 7 phosphate buffered electrolyte (B). The kinetic data were smoothed using 5-point adjacent averaging to better illustrate the trend with buffer concentration. Examples of the unsmoothed kinetic data are provided in **Figure S6**.

Independent rate constants for electron transfer and proton transfer were extracted from global fits of single wavelength kinetics collected across five wavelengths using a two-component kinetic model outlined in the supporting information. The fitting parameters and rate constants for electron and proton transfer as a function of buffer concentration are provided in **Table S2**. **Figure 5** shows the observed proton transfer rate constants (k_{PT}) plotted as a function of total buffer

concentration on a linear-log scale. At low buffer concentration, k_{PT} is independent of buffer concentration. However, at concentrations greater than 5 mM, an enhancement in k_{PT} was observed. The data were fit to expression 2 to determine the inherent rate constants for proton transfer with either water or protonated buffer serving as the proton source. Independent rate constants for ET and PT could not be satisfactorily resolved in samples where the buffer concentration exceeded 500 mM for both acetate and phosphate solutions.

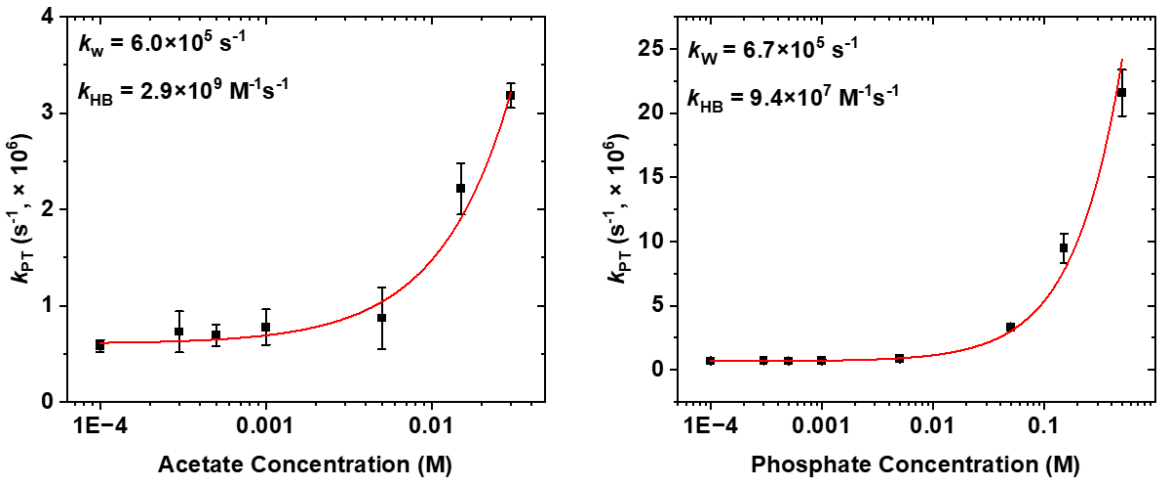

Figure 5. Plots of k_{PT} as a function of dissolved buffer ion concentration. The red lines are fits to expression 2 that was used to extract the magnitudes of k_{H2O} and k_{BH}.

Prior reports investigating the relationship between the PCET rate constants and phosphate buffer concentration for the oxidation of tyrosine have made similar observations as those noted in **Figure 5**. Therein, the concentration independent region corresponded to PCET with water as the proton donor and acceptor whereas the concentration dependent region corresponded to PCET with buffer as the primary proton donor and acceptor. The PCET kinetics in **Figure 5** can be modeled using expression 2 to determine the rate constants for proton transfer from water or buffer, respectively.

$$k_{PT} = k_w + f_{HB}[B]k_{HB} \quad (2)$$

Here, k_{PT} is the observed proton transfer rate constant obtained from fits of the time-resolved kinetics at 540 nm, k_w is the rate constant of proton transfer from bulk water (either H_2O or H_3O^+) to Ru^{III}−OH, f_{HB} is the fraction of protonated buffer at the solution pH used and is derived from the Henderson-Hasselbalch relationship, [B] is the concentration of dissolved buffer ions in solution, and k_{HB} is the rate constant of proton transfer from protonated buffer to Ru^{III}−OH. Fits of the data in **Figure 5** to expression 2 demonstrate that the rate constants for proton transfer between Ru^{III}−OH and protonated buffer is increased by two to four orders of magnitude for acetate and phosphate, respectively while the rate constant for proton transfer with water is independent of buffer identity or solution pH. In contrast to the rate constants for proton transfer, rate constants for electron transfer were found to display no significant dependence on the buffer concentration with rate constants ranging from 2.0 × 10^7 s^{-1} to 3.3 × 10^7 s^{-1}. This significant rate enhancement directly illustrates that careful selection of buffer identity and concentration can be used to dramatically enhance the kinetics of a PCET reaction.

***Discussion*.**

A well-known water oxidation catalyst was anchored to the surface of mesoporous ITO thin films. Consistent with prior studies of this catalyst either in fluid solution or anchored to the surface of ITO thin films, deprotonation of the catalyst results in a bathochromic shift in the MLCT absorption spectrum. In aqueous acetate and phosphate buffer solutions, the catalyst was shown to possess a reversible electrochemical PCET reaction associated with oxidation or reduction of the ruthenium center and corresponding protonation and deprotonation of the inner-sphere aqua ligand. When excited with visible light, the catalyst was found to inject an electron into ITO, providing a means to photo-initiate the PCET reaction. An applied potential was used to control the free energy change for interfacial electron transfer between the ITO and the oxidized catalyst while spectral changes were monitored using time-resolved absorption spectroscopy. The bathochromic shift induced upon deprotonation was used to determine the independent rate constants for ET and PT. The independent PT kinetics displayed a dependence on the concentration of dissolved buffer ions with the rates of proton transfer increasing under elevated buffer concentrations, while ET kinetics were insensitive to the buffer identity and concentration. The implications of these findings on the kinetics and mechanism of the PCET reduction of Ru^{III}−OH are discussed below with an emphasis on how buffer-base effects can be used to enhance photoelectrocatalysis.

Previous reports have considered the role of dissolved buffer ions on the kinetics and mechanisms of both electrochemical[19–23,25,26,28,31,32,51,52] and photo-initiated[36] PCET reactions. Given the slower timescale of electrochemical measurements and the inability to directly observe the independent steps of a PCET mechanism, most of these reports rely on electrochemical PCET kinetics fit to theoretical models derived for either stepwise or concerted reaction pathways. For example, the electrochemical $1e^-/1H^+$ PCET reactivity of $[Os^{II}(bpy)_2(py)OH_2]^{2+}$ where py = pyridine is well characterized and has been demonstrated to deviate from the predicted electrochemical kinetics for a stepwise reaction mechanism derived by Laviron[53–61] when $[Os^{II}(bpy)_2(py)OH_2]^{2+}$ was measured within carboxylic acid-terminated self-assembled monolayers or in pH 4.5 acetate buffer solution (2 M).[31,51,52] The deviation in the experimental electrochemical kinetics was taken as evidence to support a carboxylate-assisted change in the PCET mechanism from stepwise to concerted. Similarly, reports from Meyer *et al*, have demonstrated that the competent water oxidation catalyst, $Ru^{II}(bda)(isoq)_2$ (where bda is 2,2′-bipyridine-6,6′-dicarboxylic acid and isoq is isoquinoline), demonstrates a pronounced enhancement in the rate of water oxidation catalysis in pH 7.0 aqueous phosphate buffer solutions (0.01-0.2 M). Similar results were also obtained for catalysis performed in pH 5.6 acetate buffer solutions (0.05-0.5 M).[19] It was proposed that the presence of buffered electrolyte solutions provided concerted electron-proton transfer (EPT) pathways that enhanced the rate-limiting step of the catalytic mechanism.

Given the possibility that buffer-bases could alter the underlying PCET mechanism, it is worthwhile to re-examine the potential mechanistic pathways presented in **Scheme 2** within the context of the kinetic data presented herein. There are three generally accepted mechanisms for PCET: stepwise electron transfer-proton transfer (ET-PT), stepwise proton transfer-electron transfer (PT-ET), and concerted electron-proton transfer (EPT). In the stepwise pathways, the electron and proton are transferred in sequence whereas in EPT, both reactants are transferred in a single mechanistic step. Below, we examine each mechanism considering the kinetic and thermodynamic data presented here.

PCET via Stepwise PT-ET with Rate-Limiting PT

For stepwise PT-ET, protonation of the catalyst by the buffer prior to electron transfer would be consistent with the observed decrease in signal for Ru^{II}−OH under elevated buffer concentrations. The equilibrium constant for proton transfer between protonated buffer and Ru^{III}−OH (K_{PT} = k_{PT}/k_{-PT}) will be equal to $10^{-\Delta pK_a}$.[36] Here, the ΔpK_a for proton transfer between acetate (pK_a = 4.76) or phosphate (pK_a = 7.2) and Ru^{III}−OH (pK_a = 1.3) are 3.46 and 5.9, respectively. Assuming the rate of the reverse proton transfer can be approximated by the upper-limit for a diffusion limited protonation step ($k_{-PT} \approx k_{diff}$ = 1×10^{10} M^{-1}•s^{-1}),[62,63] the predicted bimolecular rate-constant for PT can be calculated. For acetate and phosphate buffer solutions, the predicted values of k_{PT} are 3.47×10^{6} M^{-1}•s^{-1} and 1.26×10^{4} M^{-1}•s^{-1}, respectively. These values are inconsistent the magnitudes of k_{HB} calculated from fits to the data in **Figure 5**, suggesting that a PT-ET mechanism with rate-limiting PT is unlikely. Furthermore, if PT-ET with rate-limiting PT were the operative mechanism, the PCET kinetics under elevated buffer concentrations would be expected to be independent of the driving force for electron transfer, and thus, the applied potential. Kinetic data collected as a function of V_{app} in 500 mM acetate buffer at 540 nm is provided in **Figure S7** and clearly demonstrates a dependence on the applied potential, suggesting that stepwise PT-ET with rate-limiting PT is not the operative mechanism.

PCET via Stepwise PT-ET with Rate-Limiting ET

It is possible that the PCET reduction reaction could operate via a stepwise PT-ET mechanism with rate-limiting ET. Such a mechanism would be consistent with the observed loss of signal for Ru^{II}−OH at elevated buffer concentrations while also displaying a dependence on V_{app} as ET would be the rate-limiting step. However, kinetics collected in D_2O show a primary kinetic isotope effect (KIE) of k_H/k_D of 1.5-2.0 (**Figure S8**) at all buffer concentrations investigated herein, suggesting direct proton involvement in the rate-limiting step of the mechanism.[16,64,65] As a result, stepwise PT-ET with rate-limiting ET is unlikely.

PCET via Stepwise ET-PT with Rate-Limiting PT

It was previously established that PCET under low buffer concentrations results in a stepwise ET-PT mechanism with rate-limiting PT.[42] At pH 7, under the assumption that water serves as the proton donor/acceptor at low buffer concentrations, protonation of Ru^{II}−OH to yield Ru^{II}−OH_2 is unfavorable (ΔG_{PT} = 0.22 eV) by ~5 kCal/mol. At pH 5.5, H_3O^+ and water could both potentially serve as proton donors for the PCET reaction. However, the low concentration of H_3O^+ (3.16×10^{-6} M) suggests that despite favorable thermodynamics for PT (ΔG_{PT} = −0.61 eV), the reaction is ultimately diffusion limited. Under diffusional control, the expected rate constant for proton transfer can be calculated using expression 3.

$$k_{PT} = k_{diff}[H_3O^+] \quad (3)$$

where k_{PT} is the predicted PT rate constant, k_{diff} is the diffusion-controlled bimolecular PT rate constant, and [H_3O^+] is the concentration of the presumed proton donor. In this case, hydronium ions. At pH 5.5, k_{PT} = 3.16×10^{4} s^{-1}. This value is within an order of magnitude of the rate constant obtained from fits to the kinetic data provided in **Figure 5** suggesting that small but noticeable contributions to the k_w are present due to PT from protonated buffer in solution and as a result, the values of k_w provided in **Figure 5** are likely to overestimate the true rate of PT from the bulk under these conditions. Regardless, $k_{ET} >> k_{PT}$ and results in a stepwise ET-PT mechanism with

rate-limiting PT. The direct observation of Ru^{II}−OH also provides strong evidence to support his conclusion as neither ET-PT with rate-limiting ET nor stepwise PT-ET would result in the formation and accumulation of Ru^{II}−OH. Under elevated buffer concentrations, the bimolecular PT rate constants derived from fits to expression 2 in **Figure 5** suggest that proton transfer from buffer is on the same or greater order of magnitude when compared to electron transfer ($k_{ET} \approx 1\times10^{7}$ s^{-1}). Therefore, under elevated buffer concentrations, a stepwise ET-PT mechanism with rate-limiting PT is unlikely.

PCET via Stepwise ET-PT with Rate-Limiting ET

It is possible that under elevated buffer concentrations, the rate-limiting step of the PCET mechanism shifts from PT to ET. In such a case, an ET-limited PCET reaction would imply near-instantaneous consumption of the Ru^{II}−OH intermediate, preventing its observation in time-resolved difference spectra and is consistent with the experimental results. In addition, a kinetic dependence on V_{app} would also be expected. To further probe if the kinetics under elevated buffer concentrations are indeed ET-limited, ultrafast spectroscopy was performed on samples of Ru^{II}−OH_2 in solutions of 2 M acetate buffer (pH 5.5), 800 mM phosphate buffer (pH 7), and 0.32 M $HClO_3$ (pH 0.5). Under acidic conditions where pH < pK_a = 1.3, the interfacial electron transfer reaction is no longer accompanied by deprotonation resulting in a photo-initiated reaction that is purely ET. For these measurements, V_{app} was modulated to ensure that the driving force for ET (ΔG_{ET} = −0.71 eV) was constant in all cases. The observed kinetic traces from 600 fs to 6 ns are presented in **Figure S9.** Kinetic traces measured in 2 M acetate buffer and 800 mM phosphate buffer clearly do not overlay, with the kinetics collected in pH 0.5 $HClO_4$. While this observation cannot directly rule out stepwise ET-PT with rate-limiting ET as the operative mechanism, it does suggest that the kinetics for PCET at elevated buffer concentrations are indeed slower than those for a purely ET reaction and are inconsistent with this proposed mechanism. Furthermore, we note that evidence for concerted EPT reactions occurring on ultrafast timescales was recently reported for a light-initiated multi-site PCET donor-acceptor assembly.[66]

Concerted EPT to Buffer

While it is not possible to provide direct evidence for a concerted PCET mechanism, the kinetic data herein suggest that a concerted mechanism induced by the presence of acetate or phosphate buffer is possible and could operate in parallel to a stepwise mechanism. The rationale for why a concerted EPT mechanism may occur is provided in guidelines outlined by Jencks[67] who examined case studies for complex acid-base catalyzed reactions that are able to proceed through either stepwise or concerted mechanisms. Jencks posited that for a reaction to proceed through a concerted pathway, two conditions must be met. First, there must be a large change in the pK_a of the reaction site through the course of the reaction. For $Ru^{III/II}$−OH/OH_2 ΔpK_a = 9.0 and satisfies the first criteria. Second, the pK_a of the acid-base catalyst (buffer in the examples herein) must lie between the two pK_a values of the reaction site such that it can convert an unfavorable proton transfer to a favorable one over the course of the reaction. Here, the pK_a values for acetate and dihydrogen phosphate are 4.76 and 7.2, respectively. For Ru^{III}−OH, pK_a = 1.3 and neither buffer possesses a favorable pK_a for proton transfer as discussed above for the stepwise PT-ET mechanism. However, reduction of Ru^{III}−OH to Ru^{II}−OH (pK_a = 10.3) results in favorable driving forces for proton transfer from each buffer with ΔG_{PT} = −0.33 eV and −0.18 eV for acetate and phosphate, respectively, fulling the second criteria outlined by Jencks. Within this context, the addition of acetate and phosphate buffer could provide access to rate enhancements through concerted PCET pathways.

In light of this analysis, we believe that the most likely PCET mechanisms occurring at elevated buffer concentrations are stepwise ET-PT with rate-limiting ET and/or concerted EPT. It is possible that both mechanisms are present and operate in parallel. More importantly however, these results clearly demonstrate that the addition of buffer-bases can be used to systematically control the kinetics and rate-limiting step of PCET reactions. The implications of this work are perhaps most important for photoelectrocatalysis at semiconducting interfaces where it is ideal for catalysis to be limited only by the rate interfacial electron transfer and not by the rate at which protons can be sourced from the bulk solution.

Conclusions

Associated Content

Additional experimental details, cyclic voltammograms of the catalyst in varying concentrations of buffer and solution pH, simulated transient absorption spectra, transient absorption difference spectra presented at varying buffer concentrations, single-wavelength kinetics at varying buffer concentrations and applied potentials, kinetics collected in both H_2O and D_2O, and ultrafast kinetics are provided in the electronic supporting information

Author Information

Notes

The authors declare no competing financial interests related to this work.

Acknowledgements

This material is based on work solely supported as part of the Center for Hybrid Approaches in Solar Energy to Liquid Fuels (CHASE), an Energy Innovation Hub funded by the U.S. Department of Energy, Office of Science, Office of Basic Energy Sciences, under award number DE-SC0021173. In addition, M.C.K would like to acknowledge support from the Arnold and Mabel Beckman Foundation's Postdoctoral Fellowship.

References

(1) Huynh, M. H. V.; Meyer, T. J. Proton-Coupled Electron Transfer. *Chem. Rev.* **2007**, *107* (11), 5004–5064. https://doi.org/10.1021/cr0500030.
(2) Hammes-Schiffer, S. Theory of Proton-Coupled Electron Transfer in Energy Conversion Processes. *Acc. Chem. Res.* **2009**, *42* (12), 1881–1889. https://doi.org/10.1021/ar9001284.
(3) Reece, S. Y.; Nocera, D. G. Proton-Coupled Electron Transfer in Biology: Results from Synergistic Studies in Natural and Model Systems. *Annu. Rev. Biochem.* **2009**, *78* (1), 673–699. https://doi.org/10.1146/annurev.biochem.78.080207.092132.
(4) Jenson, D. L.; Barry, B. A. Proton-Coupled Electron Transfer in Photosystem II: Proton Inventory of a Redox Active Tyrosine. *J. Am. Chem. Soc.* **2009**, *131* (30), 10567–10573. https://doi.org/10.1021/ja902896e.
(5) Gagliardi, C. J.; Vannucci, A. K.; Concepcion, J. J.; Chen, Z.; Meyer, T. J. The Role of Proton Coupled Electron Transfer in Water Oxidation. *Energy Environ. Sci.* **2012**, *5* (7), 7704. https://doi.org/10.1039/c2ee03311a.
(6) Nocera, D. G. The Artificial Leaf. *Acc. Chem. Res.* **2012**, *45* (5), 767–776. https://doi.org/10.1021/ar2003013.

(7) Reece, S. Y.; Nocera, D. G. Synergistic Studies in Natural and Model Systems: Results from Synergistic Studies in Natural and Model Systems. *Annu. Rev. Biochem.* **2015**, *78*, 673–699. https://doi.org/10.1146/annurev.biochem.78.080207.092132.Proton-Coupled.
(8) Mora, S. J.; Odella, E.; Moore, G. F.; Gust, D.; Moore, T. A.; Moore, A. L. Proton-Coupled Electron Transfer in Artificial Photosynthetic Systems. *Acc. Chem. Res.* **2018**, *51* (2), 445–453. https://doi.org/10.1021/acs.accounts.7b00491.
(9) Warburton, R. E.; Soudackov, A. V.; Hammes-Schiffer, S. Theoretical Modeling of Electrochemical Proton-Coupled Electron Transfer. *Chem. Rev.* **2022**, *122* (12), 10599–10650. https://doi.org/10.1021/acs.chemrev.1c00929.
(10) Mayer, J. M. Understanding Hydrogen Atom Transfer: From Bond Strengths to Marcus Theory. *Acc. Chem. Res.* **2011**, *44* (1), 36–46. https://doi.org/10.1021/ar100093z.
(11) McCarthy, B. D.; Dempsey, J. L. Decoding Proton-Coupled Electron Transfer with Potential–p K_a Diagrams. *Inorg. Chem.* **2017**, *56* (3), 1225–1231. https://doi.org/10.1021/acs.inorgchem.6b02325.
(12) Chalkley, M. J.; Del Castillo, T. J.; Matson, B. D.; Peters, J. C. Fe-Mediated Nitrogen Fixation with a Metallocene Mediator: Exploring p K_a Effects and Demonstrating Electrocatalysis. *J. Am. Chem. Soc.* **2018**, *140* (19), 6122–6129. https://doi.org/10.1021/jacs.8b02335.
(13) Darcy, J. W.; Koronkiewicz, B.; Parada, G. A.; Mayer, J. M. A Continuum of Proton-Coupled Electron Transfer Reactivity. *Acc. Chem. Res.* **2018**, *51* (10), 2391–2399. https://doi.org/10.1021/acs.accounts.8b00319.
(14) Liu, T.; Tyburski, R.; Wang, S.; Fernández-Terán, R.; Ott, S.; Hammarström, L. Elucidating Proton-Coupled Electron Transfer Mechanisms of Metal Hydrides with Free Energy- and Pressure-Dependent Kinetics. *J. Am. Chem. Soc.* **2019**, *141* (43), 17245–17259. https://doi.org/10.1021/jacs.9b08189.
(15) Rountree, E. S.; McCarthy, B. D.; Dempsey, J. L. Decoding Proton-Coupled Electron Transfer with Potential–p K_a Diagrams: Applications to Catalysis. *Inorg. Chem.* **2019**, *58* (10), 6647–6658. https://doi.org/10.1021/acs.inorgchem.8b03368.
(16) Tyburski, R.; Liu, T.; Glover, S. D.; Hammarström, L. Proton-Coupled Electron Transfer Guidelines, Fair and Square. *J. Am. Chem. Soc.* **2021**, *143* (2), 560–576. https://doi.org/10.1021/jacs.0c09106.
(17) Tyburski, R.; Hammarström, L. Strategies for Switching the Mechanism of Proton-Coupled Electron Transfer Reactions Illustrated by Mechanistic Zone Diagrams. *Chem. Sci.* **2022**, *13* (1), 290–301. https://doi.org/10.1039/D1SC05230F.
(18) Fertig, A. A.; Matson, E. M. Connecting Thermodynamics and Kinetics of Proton Coupled Electron Transfer at Polyoxovanadate Surfaces Using the Marcus Cross Relation. *Inorg. Chem.* **2023**, *62* (5), 1958–1967. https://doi.org/10.1021/acs.inorgchem.2c02541.
(19) Song, N.; Concepcion, J. J.; Binstead, R. A.; Rudd, J. A.; Vannucci, A. K.; Dares, C. J.; Coggins, M. K.; Meyer, T. J. Base-Enhanced Catalytic Water Oxidation by a Carboxylate–Bipyridine Ru(II) Complex. *Proc. Natl. Acad. Sci. U.S.A.* **2015**, *112* (16), 4935–4940. https://doi.org/10.1073/pnas.1500245112.
(20) Zhang, L.-H.; Yu, F.; Shi, Y.; Li, F.; Li, H. Base-Enhanced Electrochemical Water Oxidation by a Nickel Complex in Neutral Aqueous Solution. *Chem. Commun.* **2019**, *55* (43), 6122–6125. https://doi.org/10.1039/C9CC01865D.
(21) Wang, D.; Groves, J. T. Efficient Water Oxidation Catalyzed by Homogeneous Cationic Cobalt Porphyrins with Critical Roles for the Buffer Base. *Proc. Natl. Acad. Sci. U.S.A.* **2013**, *110* (39), 15579–15584. https://doi.org/10.1073/pnas.1315383110.
(22) Dong, H.; Du, J.; Kong, J.; He, X.; Chen, Z. Electrocatalytic Water Oxidation by Mononuclear Cu(II) Aliphatic Tetraamine Complexes. *ChemCatChem* **2019**, *11* (21), 5306–5312. https://doi.org/10.1002/cctc.201900033.

(23) Jeremiasse, A. W.; Hamelers, H. V. M.; Kleijn, J. M.; Buisman, C. J. N. Use of Biocompatible Buffers to Reduce the Concentration Overpotential for Hydrogen Evolution. *Environ. Sci. Technol.* **2009**, *43* (17), 6882–6887. https://doi.org/10.1021/es9008823.
(24) Jackson, M. N.; Jung, O.; Lamotte, H. C.; Surendranath, Y. Donor-Dependent Promotion of Interfacial Proton-Coupled Electron Transfer in Aqueous Electrocatalysis. *ACS Catal.* **2019**, *9* (4), 3737–3743. https://doi.org/10.1021/acscatal.9b00056.
(25) Alvarez-Hernandez, J. L.; Sopchak, A. E.; Bren, K. L. Buffer p K_a Impacts the Mechanism of Hydrogen Evolution Catalyzed by a Cobalt Porphyrin-Peptide. *Inorg. Chem.* **2020**, *59* (12), 8061–8069. https://doi.org/10.1021/acs.inorgchem.0c00362.
(26) Le, J. M.; Alachouzos, G.; Chino, M.; Frontier, A. J.; Lombardi, A.; Bren, K. L. Tuning Mechanism through Buffer Dependence of Hydrogen Evolution Catalyzed by a Cobalt Mini-Enzyme. *Biochemistry* **2020**, *59* (12), 1289–1297. https://doi.org/10.1021/acs.biochem.0c00060.
(27) Alvarez-Hernandez, J. L.; Han, J. W.; Sopchak, A. E.; Guo, Y.; Bren, K. L. Linear Free Energy Relationships in Hydrogen Evolution Catalysis by a Cobalt Tripeptide in Water. *ACS Energy Lett.* **2021**, *6* (6), 2256–2261. https://doi.org/10.1021/acsenergylett.1c00680.
(28) Schneider, C. R.; Lewis, L. C.; Shafaat, H. S. The Good, the Neutral, and the Positive: Buffer Identity Impacts CO_2 Reduction Activity by Nickel(II) Cyclam. *Dalton Trans.* **2019**, *48* (42), 15810–15821. https://doi.org/10.1039/C9DT03114F.
(29) Fecenko, C. J.; Meyer, T. J.; Thorp, H. H. Electrocatalytic Oxidation of Tyrosine by Parallel Rate-Limiting Proton Transfer and Multisite Electron−Proton Transfer. *J. Am. Chem. Soc.* **2006**, *128* (34), 11020–11021. https://doi.org/10.1021/ja061931z.
(30) Ishikita, H.; Soudackov, A. V.; Hammes-Schiffer, S. Buffer-Assisted Proton-Coupled Electron Transfer in a Model Rhenium−Tyrosine Complex. *J. Am. Chem. Soc.* **2007**, *129* (36), 11146–11152. https://doi.org/10.1021/ja072708k.
(31) Costentin, C.; Robert, M.; Savéant, J.-M.; Teillout, A.-L. Concerted Proton-Coupled Electron Transfers in Aquo/Hydroxo/Oxo Metal Complexes: Electrochemistry of $[Os^{II}(Bpy)_2Py(OH_2)]^{2+}$ in Water. *Proc. Natl. Acad. Sci. U.S.A.* **2009**, *106* (29), 11829–11836. https://doi.org/10.1073/pnas.0905020106.
(32) Chen, Z.; Concepcion, J. J.; Hu, X.; Yang, W.; Hoertz, P. G.; Meyer, T. J. Concerted O Atom–Proton Transfer in the O—O Bond Forming Step in Water Oxidation. *Proc. Natl. Acad. Sci. U.S.A.* **2010**, *107* (16), 7225–7229. https://doi.org/10.1073/pnas.1001132107.
(33) Costentin, C. Electrochemical Approach to the Mechanistic Study of Proton-Coupled Electron Transfer. *Chem. Rev.* **2008**, *108* (7), 2145–2179. https://doi.org/10.1021/cr068065t.
(34) Costentin, C.; Robert, M.; Saveant, J. M. Update 1 of: Electrochemical Approach to the Mechanistic Study of Proton-Coupled Electron Transfer. *Chemical Reviews* **2010**, *110* (12), PR1–PR40. https://doi.org/10.1021/cr100038y.
(35) Savéant, J. M. Electrochemical Approach to Proton-Coupled Electron Transfers: Recent Advances. *Energy and Environmental Science* **2012**, *5* (7), 7718–7731. https://doi.org/10.1039/c2ee03241d.
(36) Irebo, T.; Reece, S. Y.; Sjödin, M.; Nocera, D. G.; Hammarstrom, L. Proton-Coupled Electron Transfer of Tyrosine Oxidation: Buffer Dependence and Parallel Mechanisms. *Journal of the American Chemical Society* **2007**, *129* (50), 15462–15464. https://doi.org/10.1021/ja073012u.
(37) Lyon, L. A.; Hupp, J. T. Energetics of the Nanocrystalline Titanium Dioxide/Aqueous Solution Interface: Approximate Conduction Band Edge Variations between $H_0 = -10$ and $H_- = +26$. *J. Phys. Chem. B* **1999**, *103* (22), 4623–4628. https://doi.org/10.1021/jp9908404.

(38) Schrauben, J. N.; Hayoun, R.; Valdez, C. N.; Braten, M.; Fridley, L.; Mayer, J. M. Titanium and Zinc Oxide Nanoparticles Are Proton-Coupled Electron Transfer Agents. *Science* **2012**, *336* (6086), 1298–1301. https://doi.org/10.1126/science.1220234.
(39) Castillo-lora, J.; Delley, M. F.; Laga, S. M.; Mayer, J. M. Two-Electron − Two-Proton Transfer from Colloidal ZnO and TiO 2 Nanoparticles to Molecular Substrates. *J. Phys. Chem. Lett.* **2020**, *11* (18), 7687–7691. https://doi.org/10.1021/acs.jpclett.0c02359.
(40) Fertig, A. A.; Brennessel, W. W.; McKone, J. R.; Matson, E. M. Concerted Multiproton–Multielectron Transfer for the Reduction of O $_2$ to H $_2$ O with a Polyoxovanadate Cluster. *J. Am. Chem. Soc.* **2021**, *143* (38), 15756–15768. https://doi.org/10.1021/jacs.1c07076.
(41) Mayer, J. M. Bonds over Electrons: Proton Coupled Electron Transfer at Solid–Solution Interfaces. *J. Am. Chem. Soc.* **2023**, *145* (13), 7050–7064. https://doi.org/10.1021/jacs.2c10212.
(42) Kessinger, M. C.; Xu, J.; Cui, K.; Loague, Q.; Soudackov, A. V.; Hammes-Schiffer, S.; Meyer, G. J. Direct Evidence for a Sequential Electron Transfer–Proton Transfer Mechanism in the PCET Reduction of a Metal Hydroxide Catalyst. *J. Am. Chem. Soc.* **2024**, *146* (3), 1742–1747. https://doi.org/10.1021/jacs.3c10742.
(43) Kessinger, M.; Soudackov, A. V.; Schneider, J.; Bangle, R. E.; Hammes-Schiffer, S.; Meyer, G. J. Reorganization Energies for Interfacial Proton-Coupled Electron Transfer to a Water Oxidation Catalyst. *J. Am. Chem. Soc.* **2022**, *144* (44), 20514–20524. https://doi.org/10.1021/jacs.2c09672.
(44) Bard, A. J.; Faulkner, L. R. *Electrochemical Methods: Fundamentals and Applications*, 2nd ed.; Wiley: New York, 2001.
(45) Wasylenko, D. J.; Ganesamoorthy, C.; Koivisto, B. D.; Henderson, M. A.; Berlinguette, C. P. Insight into Water Oxidation by Mononuclear Polypyridyl Ru Catalysts. *Inorg. Chem.* **2010**, *49* (5), 2202–2209. https://doi.org/10.1021/ic902024s.
(46) Farnum, B. H.; Morseth, Z. A.; Brennaman, M. K.; Papanikolas, J. M.; Meyer, T. J. Application of Degenerately Doped Metal Oxides in the Study of Photoinduced Interfacial Electron Transfer. *J. Phys. Chem. B* **2015**, *119* (24), 7698–7711. https://doi.org/10.1021/jp512624u.
(47) Bangle, R. E.; Schneider, J.; Piechota, E. J.; Troian-Gautier, L.; Meyer, G. J. Electron Transfer Reorganization Energies in the Electrode-Electrolyte Double Layer. *J. Am. Chem. Soc.* **2020**, *142* (2), 674–679. https://doi.org/10.1021/jacs.9b11815.
(48) Schneider, J.; Bangle, R. E.; Swords, W. B.; Troian-Gautier, L.; Meyer, G. J. Determination of Proton-Coupled Electron Transfer Reorganization Energies with Application to Water Oxidation Catalysts. *J. Am. Chem. Soc.* **2019**, *141* (25), 9758–9763. https://doi.org/10.1021/jacs.9b01296.
(49) Farnum, B. H.; Morseth, Z. A.; Lapides, A. M.; Rieth, A. J.; Hoertz, P. G.; Brennaman, M. K.; Papanikolas, J. M.; Meyer, T. J. Photoinduced Interfacial Electron Transfer within a Mesoporous Transparent Conducting Oxide Film. *J. Am. Chem. Soc.* **2014**, *136* (6), 2208–2211. https://doi.org/10.1021/ja4106418.
(50) Concepcion, J. J.; Jurss, J. W.; Templeton, J. L.; Meyer, T. J. One Site Is Enough. Catalytic Water Oxidation by [Ru(Tpy)(Bpm)(OH 2)]2+ and [Ru(Tpy)(Bpz)(OH2)]2+. *J. Am. Chem. Soc.* **2008**, *130* (49), 16462–16463. https://doi.org/10.1021/ja8059649.
(51) Haddox, R. M.; Finklea, H. O. Proton-Coupled Electron Transfer of an Osmium Aquo Complex on a Self-Assembled Monolayer on Gold. *J. Phys. Chem. B* **2004**, *108* (5), 1694–1700. https://doi.org/10.1021/jp035967e.
(52) Madhiri, N.; Finklea, H. O. Potential-, pH-, and Isotope-Dependence of Proton-Coupled Electron Transfer of an Osmium Aquo Complex Attached to an Electrode. *Langmuir* **2006**, *22* (25), 10643–10651. https://doi.org/10.1021/la061103j.
(53) Laviron, E. Theoretical Study of a 1e, 1H+ Surface Electrochemical Reaction (Four-Member Square Scheme) When the Protonation Reactions Are at Equilibrium. *Journal of*

Electroanalytical Chemistry and Interfacial Electrochemistry **1980**, *109* (1–3), 57–67. https://doi.org/10.1016/S0022-0728(80)80106-9.
(54) Laviron, E. Electrochemical Reactions with Protonations at Equilibrium: Part II. The 1e, 1H+ Reaction (Four-Member Square Scheme for a Heterogeneous Reaction). *Journal of Electroanalytical Chemistry and Interfacial Electrochemistry* **1981**, *124* (1–2), 1–7. https://doi.org/10.1016/S0022-0728(81)80280-X.
(55) Laviron, E. Electrochemical Reactions with Protonations at Equilibrium: Part III. The 1e, 2H+ Reaction (Six-Member Ladder Scheme) for a Surface or for a Heterogeneous Reaction. *Journal of Electroanalytical Chemistry and Interfacial Electrochemistry* **1981**, *124* (1–2), 9–17. https://doi.org/10.1016/S0022-0728(81)80281-1.
(56) Laviron, E. Electrochemical Reactions with Protonations at Equilibrium Part V. The 1 e, 1 H+ Homogeneous Isotopic Exchange Reaction. *Journal of Electroanalytical Chemistry and Interfacial Electrochemistry* **1982**, *134* (2), 205–212. https://doi.org/10.1016/0022-0728(82)80001-6.
(57) Laviron, E. Electrochemical Reactions with Protonations at Equilibrium: Part VII. The 2e, 1H+ Reaction (Six-Member Fence Scheme) for a Surface or for a Heterogeneous Reaction in the Absence of Disproportionation or Dimerization. *Journal of Electroanalytical Chemistry and Interfacial Electrochemistry* **1983**, *146* (1), 1–13. https://doi.org/10.1016/S0022-0728(83)80109-0.
(58) Laviron, E. Electrochemical Reactions with Protonations at Equilibrium: Part VIII. The 2e, 2H+ Reaction (Nine-Member Square Scheme) for a Surface or for a Heterogeneous Reaction in the Absence of Disproportionation and Dimerization Reactions. *Journal of Electroanalytical Chemistry and Interfacial Electrochemistry* **1983**, *146* (1), 15–36. https://doi.org/10.1016/S0022-0728(83)80110-7.
(59) Laviron, E. Electrochemical Reactions with Protonations at Equilibrium: Part X. The Kinetics of the p-Benzoquinone/Hydroquinone Couple on a Platinum Electrode. *Journal of Electroanalytical Chemistry and Interfacial Electrochemistry* **1984**, *164* (2), 213–227. https://doi.org/10.1016/S0022-0728(84)80207-7.
(60) Laviron, E. Electrochemical Reactions with Protonations at Equilibrium: Part XI. The 1e, 2H+ Homogeneous Isotopic Electron Exchange Reaction (Six-Member Ladder Scheme). *Journal of Electroanalytical Chemistry and Interfacial Electrochemistry* **1984**, *169* (1–2), 23–28. https://doi.org/10.1016/0022-0728(84)80070-4.
(61) Laviron, E. Electrochemical Reactions with Protonations at Equilibrium: Part XII. The 2e, 2H+ Homogeneous Isotopic Electron Exchange Reaction (Nine-Member Square Scheme). *Journal of Electroanalytical Chemistry and Interfacial Electrochemistry* **1984**, *169* (1–2), 29–46. https://doi.org/10.1016/0022-0728(84)80071-6.
(62) Eigen, M.; Hammes, G. G. Elementary Steps in Enzyme Reactions (as Studied by Relaxation Spectrometry). In *Advances in Enzymology - and Related Areas of Molecular Biology*; Nord, F. F., Ed.; Wiley, 1963; Vol. 25, pp 1–38. https://doi.org/10.1002/9780470122709.ch1.
(63) Koenig, S. H.; Brown, R. D. H_2CO_3 as Substrate for Carbonic Anhydrase in the Dehydration of HCO_3^-. *Proc. Natl. Acad. Sci. U.S.A.* **1972**, *69* (9), 2422–2425. https://doi.org/10.1073/pnas.69.9.2422.
(64) Nomrowski, J.; Wenger, O. S. Photoinduced PCET in Ruthenium–Phenol Systems: Thermodynamic Equivalence of Uni- and Bidirectional Reactions. *Inorg. Chem.* **2015**, *54* (7), 3680–3687. https://doi.org/10.1021/acs.inorgchem.5b00318.
(65) Pannwitz, A.; Wenger, O. S. Photoinduced Electron Transfer Coupled to Donor Deprotonation and Acceptor Protonation in a Molecular Triad Mimicking Photosystem II. *J. Am. Chem. Soc.* **2017**, *139* (38), 13308–13311. https://doi.org/10.1021/jacs.7b08761.
(66) Arsenault, E. A.; Guerra, W. D.; Shee, J.; Reyes Cruz, E. A.; Yoneda, Y.; Wadsworth, B. L.; Odella, E.; Urrutia, M. N.; Kodis, G.; Moore, G. F.; Head-Gordon, M.; Moore, A. L.;

Moore, T. A.; Fleming, G. R. Concerted Electron-Nuclear Motion in Proton-Coupled Electron Transfer-Driven Grotthuss-Type Proton Translocation. *J. Phys. Chem. Lett.* **2022**, *13* (20), 4479–4485. https://doi.org/10.1021/acs.jpclett.2c00585.
(67) Jencks, W. P. Requirements for General Acid-Base Catalysis of Complex Reactions. *J. Am. Chem. Soc.* **1972**, *94* (13), 4731–4732. https://doi.org/10.1021/ja00768a052.